JOURNAL OF OPTOELECTRONICS AND ADVANCED MATERIALS, Vol. 10, No. 12, December 2008, p. 3300 - 3304

Synthesis, structural analysis and magnetic properties of Sc-doped $Nd_{0.8}Sr_{0.2}Mn_{1-x}Sc_xO_3$ manganites

N. CORNEI, C. MITA, O. MENTRE[a], F. ABRAHAM[b], M.-L. CRAUS[b,c*]
Chemistry Department, "Al.I.Cuza"University, Iassy, Romania
[a]*UCCS, Equipe de Chimie du Solide, ENSCL, Lille, France*
[b]*National Institute of R&D for Technical Physics, Iassy, Romania*
[c]*Joint Institute of Nuclear Research, Dubna, Russia*

A new type of manganites ($Nd_{0.8}Sr_{0.2}Mn_{1-x}Sc_xO_3$) were obtained by sol-gel method. Chemical composition was obtained by means of EDX method. The thermogravimetric analysis put in evidence two changes in DTA and TG curves, which was attributed to loss of the oxygen. XRD analysis was performed with a Huber diffractometer at room temperature, data being handled using the Rietveld refinement method. The samples contain only an orthorhombic (Pnma) phase. The magnetic measurements were performed from 4 to 350 K with a Maglab EXA9T magnetometer. A decrease of the Curie temperature with the increase of Sc concentration in the samples was observed.

(Received September 9, 2008; accepted November 27, 2008)

Keywords: Manganites, X-ray diffraction, Magnetic properties, Magnetoresistance

1. Introduction

Mixed-valence perovskite manganites $R_{1-x}A_xMnO_3$ (R = rare-earth element, A = divalent alkaline earth element) with colossal magnetoresistance effect have been of great interest in the past years due to their special electronic and magnetic properties as well as the potential utility for application [1–3].

The electrical and magnetic properties of doped manganites are controlled by the amount of doping and the tolerance factor [4]. Remarkably, paramagnetic insulator, ferromagnetic–metallic, and charge ordered–insulator temperature-dependent phase transitions are induced in the doped manganites. A colossal negative magnetoresistance, which has attracted increasing interest in the last decade [5], is observed near either the concomitant paramagnetic insulator–ferromagnetic metallic phase transition [6] or the ferromagnetic metallic–charge ordered insulator transition [7].

A large number of reports have shown that substitution at the A (Ca, Sr, Ba, Pb, etc) or B (3d elements) sites can significantly modify the MR due to the influence on the double-exchange (DE) interaction of distortion in the Mn^{3+}–O^{2-}–Mn^{4+} network or through magnetic coupling between the dopant and Mn ions [8-10]. Local distortions of the MnO_6 octahedra determine the charge transport behavior and complex magnetic and crystalline structures.

Li *et al.* have investigated magnetotransport behavior in $La_{0.7}Sr_{0.3}Mn_{0.9}M_{0.1}O_3$ (M=Cr, Fe,Ni, Cu) nanoscaled polycrystals and found an enhanced low-field magnetoresistance in the B-site-doped manganites with a direct impact on the DE interaction [8]. In general, the substitution of Mn ions suppresses the long-range ferromagnetic (FM) order. It has been well documented that partial substitution at the Mn site of other transition metal ions can greatly reduce the Curie temperature *(T_C)* and enhance the MR. According to the DE mechanism, the Mn^{3+}–O^{2-}–Mn^{4+} network is the key parameter in controlling the magnetic/transport behaviors. The larger the variation in the Mn^{3+}–O^{2-}–Mn^{4+} network, the greater the modification in the MR. Scandium is a special element among 3d transition metal ions because of having the largest ionic radius. A large lattice effect arising from Sc^{3+} on magnetic and transport properties was observed in the $La_{0.7}Ca_{0.3}MnO_3$ system [11]. As has been demonstrated, $La_{0.7}Sr_{0.3}MnO_3$ has a high T_C of about 370 K that could be decreased to room temperature by partial replacement of Mn ions. In this paper, we focused on the obtaining of $Nd_{0.8}Sr_{0.2}Mn_{1-x}Sc_xO_3$ manganites and the determination of the influence of the Sc cations on the structure and the magnetic properties.

2. Experimental

The samples with the chemical composition $Nd_{0.8}Sr_{0.2}Mn_{1-x}Sc_xO_3$ (NSMSO) (x = 0.0; 0.1) were prepared by means of sol-gel method. The stoichiometric amounts of analytical reagents of $Nd(NO_3)_3 \cdot 6H_2O$, $Sr(NO_3)_2 \cdot 7H_2O$, $MnCl_2 \cdot 4H_2O$ and Sc_2O_3 were dissolved in dilute HNO_3 (1N) solution. Suitable amounts of glycol as chelating agents were added and a homogeneous transparent solution was achieved. The solution was heated, a brown gel being obtained. The gel was preheated in air at 800 ºC for 15 h to remove the remaining organic materials and then annealed at 1150 ºC for 24 h. To determine the decomposition temperature of the gel, few

samples were subjected to a thermal analysis (TG, DTG, DTA) (s. Fig. 1).

The thermal decomposition of the gel takes place in four distinct stages: I) loss of water molecules (adsorbed or intercalated) (80-150ºC); II) dehydroxylation, decomposition of organic molecules and loss of the volatile anion (150ºC - 300ºC) ; III) loss of the reduced carbon and NO_2^- groups (300ºC - 900ºC); and IV) total elimination of the carbon, loss of the oxygen and formation of the pure perovskite structure (900-1200 ºC) (Fig. 1). The percent of mass lost till 1000 ºC is bigger for the samples with large amount of Sc. The DTG curves show an abrupt slope for the I and II stages, the shape of first minimum DTG peak gives an indication of the kinetic involved in the elimination of water molecules. The existence and strength of hydrogen bonds from the precursor gel are determined by the radius and electronegativity of the metallic elements.

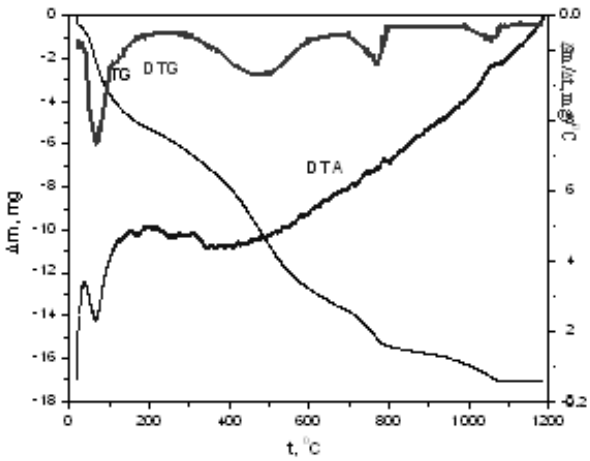

Fig. 1. TG/DTG curves for NSMSO manganite.

The presence of Sc in the perovskite was checked by EDS analysis. The presintered and sintered samples were monitorized by X-ray analysis, to determine begin of the solid-state reaction and the phase composition. XRD analysis was performed with a Huber diffractometer at room temperature, data being handled by FULLPROF 2000 [12]. Magnetic measurements were performed between 4 and 350 K with a OXFORD Maglab EXA 9T magnetometer.

The Mn-O distances, Mn-O-Mn angles, have been calculated from the atomic coordinates in the unit cell and stay at the basis of our further discussion.

3. Results and discussion

The sintered samples contain only a phase, which have an orthorhombic structure (SG 62 – Pnma) (s. Fig 2), in agreement with the literature [13, 14]. For the magnetic properties we measured only the pure samples. The cell parameters have been refined through the profile matching stage of the Rietveld refinement (Fig. 2 and Table 1). In second stage atoms positions and occupancies have been refined on the basis of data from the literature. The cationic nature in mixed occupied positions has been validated by the stoechiometry and the values of thermal parameters. The final atomic positions and isotropic temperature factors are reported in Table 2. The final R value are presented in figure 2(a, b), according to the pertinence of the proposed models.

The manganite structure is formed by chains of MnO_6 octhaedra. Between the MnO_6 octhaedra are sitting A cations, twelve coordinated with oxygen (s. Fig. 3). The unit cell volume increases with the decrease of the Mn/Sc ratio. (Table 1).

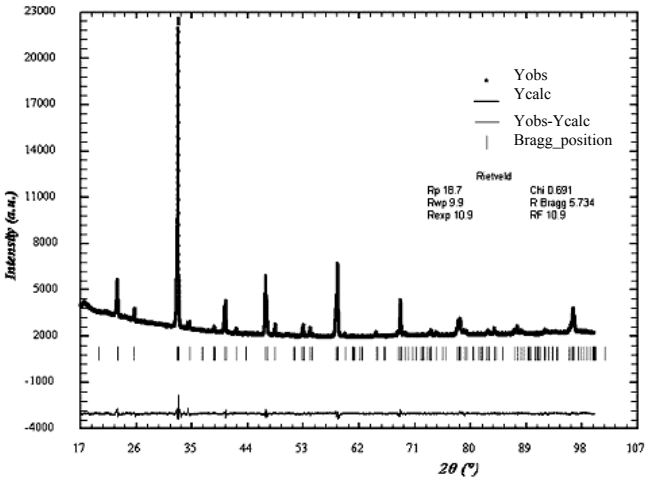

a

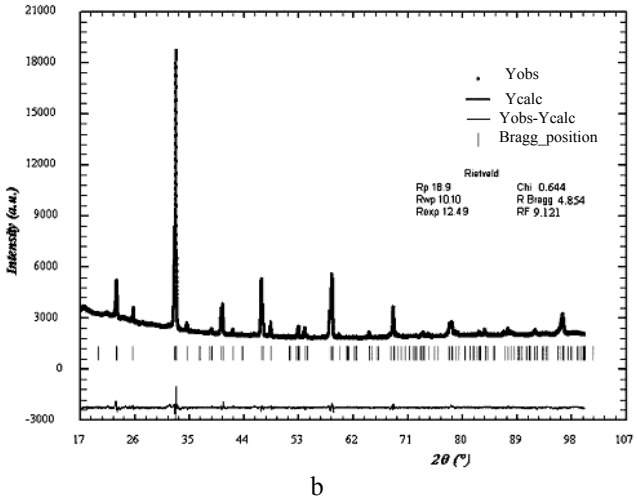

b

Fig. 2. The observed, calculated and difference difractograms of the NSMSO manganites: a) x=0.0 and b) x=0.1

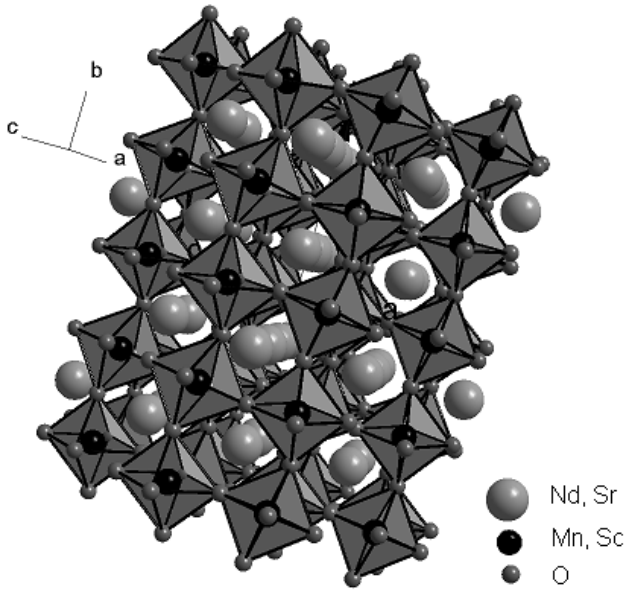

Fig. 3. $Mn(Sc)O_6$ octhaedra chains and Mn-O-Mn chains in orthorhombic structure of NSMSO.

This is consistent with the fact that the radius of Sc^{3+} (0.885 Å) is much larger than that of Mn^{3+} (0.785 Å), and obeys the trend already reported in the literature [13, 14]. We have defined the octahedral distortion as being:

$$\Delta = \frac{\left|\langle d^{ap}_{Mn-O}\rangle - \langle d^{eq}_{Mn-O}\rangle\right|}{\langle d^{ap}_{Mn-O}\rangle} \qquad (1)$$

where: 1) d^{ap}_{Mn-O} is the distance between the Mn (Sc) cations and O1 anions, which are sitting on the (4b) sites, respectively, on (4c) sites and 2) d^{eq}_{Mn-O} - the distance between Mn, on (4b) sites, and O2, on (8d) sites in the unit cell.

Table 1. Dependence of the lattice constants (a, b, c), unit cell volume (V) and the tolerance factor (t) with the Sc concentration (x) in NSMSO.

x	a(Å)	b(Å)	c(Å)	V(Å^3)	t
0.0	5.4925	7.7076	5.4572	231.03	0.901
0.1	5.5022	7.7082	5.4556	231.38	0.914

The double/super-exchange (DE/SE) interactions between the Mn cations was correlated with the band width, given by the relation:

$$w \propto \frac{\cos(\frac{1}{2}(\pi - \angle Mn - O - Mn))}{\langle d_{Mn-O}\rangle^{3.5}} \qquad (2)$$

An increase of the distortion degree of the MnO_6 octahedra takes place with the increase of Sc concentration in the samples (s.Tab.3). This behavior could be attributed to the substitution of Mn^{3+} cations (r_{Mn3+}=0.785 Å) with Sc^{3+} cations (r_{Sc3+}=0.885 Å), although the scandium cations are not Jahn-Teller cations.

Table 2. Atomic positions and equivalent isotropic displacement parameters (B_{eq}) for NSMSO.

x	Atom	Site	x, y, z	B_{eq} (Å^2)	Occ
0.0	Nd	4c	0.03487_{26} 0.25000_{0} -0.00741_{60}	0.564_{38}	0.8
	Sr	4c	0.03487_{26} 0.25000_{0} -0.00741_{60}	0.564_{38}	0.2
	Mn	4b	0.0000_{0} 0.0000_{0} 0.5000_{0}	0.288_{63}	1
	O1	4c	0.49381_{160} 0.2500_{0} 0.06550_{246}	1.307_{134}	1
	O2	8d	0.27485_{260} 0.04477_{179} 0.70148_{156}	1.307_{134}	1
0.10	Nd	4c	0.03602_{8} 0.2500_{0} -0.00493_{41}	0.747_{14}	0.8
	Sr	4c	0.03602_{8} 0.25000_{0} -0.00493_{41}	0.747_{14}	0.2
	Mn	4b	0.0000_{0} 0.0000_{0} 0.5000_{0}	0.180_{21}	0.9
	Sc	4b	0.0000_{0} 0.0000_{0} 0.5000_{0}	0.180_{21}	0.1
	O1	4c	0.49459_{99} 0.25000_{0} 0.08120_{8}	1.370_{88}	1
	O2	8d	0.28873_{88} 0.02960_{102} 0.72976_{148}	1.370_{88}	1

Note: Equivalent isotropic temperature factors are computed according to the relation $Beq = 4/3\Sigma_{ij}\beta_{ij}a_ia_j$.

Table 3. Variation of Mn-O average distances ⟨d_{Mn-O}⟩, Mn-O-Mn bonds average angles (⟨∠ Mn-O-Mn⟩), MnO_6 octhaedra distortion (Δ) and of the band width (w) with Sc concentration (x)

x	⟨d_{Mn-O}⟩	⟨∠ $\theta_{Mn-O-Mn}$⟩	Δ	w
0.00	1.960_0(ap) 1.879_0(eq)	158.889_1(ap) 159.422_6(eq)	0.041	0.103
0.10	1.976_0(ap) 1.891_0(eq)	154.360_0(ap) 160.875_4(eq)	0.043	0.100

We suppose that the cation distribution in the investigated compounds is given by the formula:

$$(Nd^{3+}_{0.8}Sr^{2+}_{0.2})_A(Mn^{4+}_{0.2}Mn^{3+}_{0.8-x}Sc^{3+}_{x})_B O_3 \qquad (3)$$

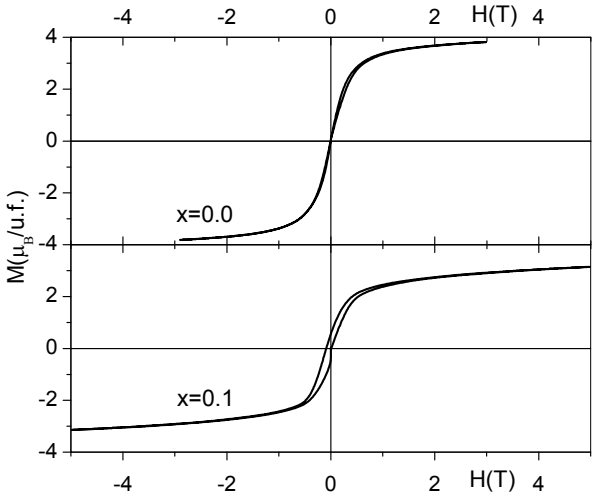

Fig. 4 Magnetization dependence on magnetic field and Sc concentration in NSMSO manganites at 4K.

In agreement with Eq.(3) and the atomic moments of Mn^{3+} (S = 2, M_S= 4μ_B) and Mn^{4+} (S = 3/2, M_S = 3μ_B) the molecular magnetic moments should decrease with the increase of Sc concentration on B places (s.Tab.4).

Table 4 The variation of observed specific and molar magnetization (σ, p), of the calculated molar magnetization (p_{calc}) and of the Curie temperature (T_C).

x	σ (uem/g)	M*(μ_B/f.u.)	p_{calc}(μ_B/f.u.)	T_C(K)*)
0.00	80.6	3.78	3.8	162.2
0.10	57.6	3.18	3.4	135.7

*)determined from the variation of magnetization with the intensity of magnetic field at low temperature (s.Fig. 4)
**)determined from the variation of the susceptibility with the temperature (s.Fig. 5)

A good agreement there is between the observed magnetic moments (s. Fig. 4) and the calculated magnetic moments, considering only the contribution of the manganese to the magnetic structure of manganites.

We can conclude that, even at low temperature, the magnetic moment of Nd has no contribution to the specific magnetization of the samples.

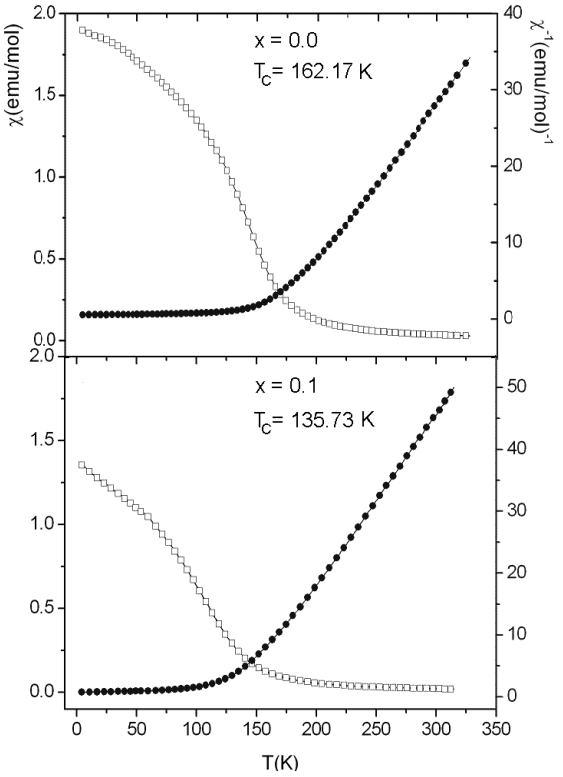

Fig. 5. Variation of susceptibility vs. temperature for NSMSO manganites.

Concerning the magnetic interaction between the manganese cations, we observe a decrease of the $\langle\angle\ \theta_{Mn\text{-}O\text{-}Mn}\rangle$ angles and an increase of the $\langle d_{Mn\text{-}O}\rangle$ distances, which should leads to a decrease of the double exchange interaction. This observation agrees with the values of the Curie temperature (determined from the variation of the susceptibility with the temperature (s. Fig.5)) and with the calculated values of the bandwidth (s.Tab.3). In addition, from the effective moments deduced from the paramagnetic domains (T>Tc) are in relatively good agreement with the general formula it given in the equation (3). For x = 0 and 0.1, the experimental Curie constant C are 4.92 and 3.59 emu.K.mol^{-1} respectively while it is calculated to 4.41 and 4.10. For this calculation, we used:

$$C = \Sigma_i\, n_i\, C_i \qquad (4)$$

where n_i is the stoichiometric coefficient for the element i and C_i is calculated within a spin-only approximation for Mn^{3+} and Mn^{4+} ($C_i = S_i(S_i+1)/2$) and considering the spin-orbit coupling for Nd^{3+} ($C_i = g_i^2\,(J_i)(J_i+1)/8$). The smallest experimental values could picture some degree of spin orbit coupling for the manganese.

It is known that the substitution of the Mn with Ga, Sc or Al in some manganites as $LaMn_{1-x}Ga_xO_3$, $LaMn_{1-x}Sc_xO_3$ or $LaMn_{1-x}Al_xO_3$ leads to apparition of the spin-glass behavior [13, 14]. The $LaMnO_3$ is antiferromagnetic, but the substitution of Mn with cations as Ga, Sc or Al, even for a small concentration, leads to an isolation of Mn cations [13].

In the present system, the substitution of Mn with Sc diminishes the double exchange interaction, but apparently did not induce a spin-glass behavior.

4. Conclusions

We had prepared $Nd_{0.8}Sr_{0.2}Mn_{1-x}Sc_xO_3$ manganites (x=0 and 0.1) by sol-gel methods. For a low concentration of Sc pure orthorhombic manganites were obtained. The substitution of Mn with Sc leads to an increase of the unit cell volume, an increase of the average Mn-O distances and to a decrease of Mn-O-Mn bond angles. The DE interaction decreases for higher concentration of the Sc, observed consequences being a decrease of the Curie temperature and of the specific/molar magnetization. No contribution of Nd magnetic moment to the total magnetic moment, even at low temperature, was observed.

References

[1] C. Zener, Phys. Rev. **82,** 403 (1951).
[2] R. von Helmolt, J. Wecker, B. Holzapfel, L. Schultz, K. Samwer,, Phys. Rev. Lett. **71,** 2331 (1993).
[3] M. Pissas, G. Kallias, Phys. Rev. **B 68,** 134414 (2003).
[4] P. M. Woodward, T. Vogt, D. E. Cox, A. Arulraj, C. N. R. Rao, P. Karen, A. K. Cheetham, Chem. Mater. **10,** 3652 (1998)
[5] A. P. Ramirez, J. Phys: Condens. Matter **9**, 8171 (1997).
[6] J. M. D. Coey, M. Viret, S. von Molnar, Adv. Phys. **48**, 167 (1999)**.**
[7] C. Kapusta, P.C. Riedi, M. Sikora, M. R. Ibarra, Phys. Rev. Lett. **84,** 4216 (2000).
[8] X. H. Li, Y. H. Huang, C. H. Yan, Z. M. Wang, C. S. Liao, J. Phys.: Condens. Matter 14, L177 (2002)
[9] F. Chen, H. W. Liu, K. F. Wang, H. Yu, S. Dong, X. Y. Chen, X. P. Jiang, Z. F. Ren, J-M Liu J. Phys.: Condens. Matter **17,** L467 (2005).
[10] J. Gutierrez, F. J. Bermejo, N. Veglio, J. M. Barandiarán, P. Romano, C. Mondelli, M. A. González and A. P. Murani, J. Phys.: Condens. Matter **18,** 9951 (2006).
[11] Y. H. Huang, C. S. Liao, Z. M. Wang, X. H. Li, C. H. Yan, J. R. Sun, B. G. Shen, Phys. Rev. B **65 (**2002)184423.
[12] T. Roisnel, J. Rodriguez-Carvajal, WinPLOTR: a Windows tool for powder diffraction patterns analysis Materials Science Forum, Proceedings of the Seventh European Powder Diffraction Conference (EPDIC 7), Ed. R. Delhez and E.J. Mittenmeijer, 2000, 118-123
[13] J. B. Goodenough, R. I. Dass, J. Zhou, Solid State Sciences **4,** 297 (2002).
[14] Y. -H. Huang, C. -H. Yan, X. -H. Li, F. Luo, C.-S. Liao, Z. -M. Wang, J. Phys.: Condens. Matter **14,** 10316 (2002).

*Corresponding author: mihailliviu@yahoo.com